PCCP

Accepted Manuscript

ROYAL SOCIETY OF CHEMISTRY

www.rsc.org/pccp

PCCP

RSCPublishing

PERSPECTIVE

Promising anchoring groups for single-molecule conductance measurements

Cite this: DOI: 10.1039/x0xx00000x

Received xxth January 2014,
Accepted xxth xxxxxxx

DOI: 10.1039/x0xx00000x

www.rsc.org/

Veerabhadrarao Kaliginedi,[a]* Alexander Rudnev,[a] Pavel Moreno-García,[a] Masoud Baghernejad,[a] Cancan Huang,[a] Wenjing Hong,[a]* and Thomas Wandlowski[a]

The understanding of the charge transport through single molecule junctions is a prerequisite for design and building of electronic circuits based on single molecule junctions. However, reliable and robust formation of such junctions is a challenging task to achieve. In this topical review, we present a systematic investigation of anchoring group effect on single molecule junction conductance by employing two complementary techniques, namely scanning tunneling microscopy break junction (STM-BJ) and mechanically controlled break junction (MCBJ) techniques, based on the studies published in literature and important results from our own work. We compared conductance studies for conventional anchoring groups described earlier with the molecular junctions formed through π-interactions with the electrode surface (Au, Pt, Ag) and we also summarized recent development to form highly conducting covalent Au-C σ-bonds using oligophenyleneethynylene (OPE) and alkane molecular backbone. Specifically, we focus on the electron transport properties of diaryloligoyne, oligophenyleneethynylene (OPE) and/or alkane molecular junctions composing of several traditional anchoring groups, (dihydrobenzo[b]thiophene (BT), 5-benzothienyl analogue (BTh), thiol (SH), pyridyl (PY), amine (NH_2), cyano (CN), methyl sulphide (SMe), nitro (NO_2)) and other anchoring groups at solid/liquid interface. The qualitative and quantitative comparison of the results obtained with different anchoring groups reveals structural and mechanistic details of the different types of single molecular junctions. The results reported in this prospective may serve as a guideline for the design and the synthesis of molecular systems to be used in molecule-based electronic devices.

Introduction

The idea of building electronic devices using single molecules as active components was first proposed by Aviram and Ratner in 1974.[1] Indeed, molecules are of great interest for application in electronic devices because of their small size, recognition properties, unique ability to self-assembly (specific/highly selective interactions) and versatility of their chemical modification and/or customization.[2] Thus, the ability to measure and control charge transport across metal/molecule/metal junction is of considerable fundamental interest and represents a key step towards the development of single-molecule electronic devices.

For the last two decades many research groups across the world have been developing several techniques to understand and to characterize the charge transport through molecular junctions formed by a single molecule or an ensemble of molecules.[3-5] In the ensemble approach, a molecular monolayer is typically sandwiched between two electrodes,[6] which can be liquid as in metal junctions employing either mercury (Hg)[7] or gallium-indium eutectic alloy (EGaIn),[8] or solid as in cross wire junctions,[9] nanopores,[10] and Au colloid arrays.[11] A detailed description of such arrangements is found in comprehensive reviews.[3, 4] In contrast, conductance experiments with few or single molecule junctions have been addressed in matrix isolation experiments,[12] mechanically controllable break junction experiments (MCBJ),[5, 13] scanning probe microscopy break junctions (STM-BJ and CP-AFM-BJ)[14-18] and related techniques.[19-22] The aforementioned techniques have enabled the understanding of structure-property correlations in single molecular electronics[23-32] including anchoring group effect,[17, 33-

[35] length dependence,[36-38] and quantum interference effect.[21, 39-41]

A critical issue in all these experimental studies is the formation of a reliable electrical contact between the target molecules and the macroscopic electrodes surface. Therefore, it is very important to understand the effect of anchoring group on the electron transport through the molecular junction. In this prospective we will discuss some of the important experimental results published in literature on anchoring group effect on single molecular junction conductance. Due to the different experimental conditions, techniques and data analysis procedure adopted by the research groups across the world, it is very hard to compare the experimental results obtained by different groups on one to one basis. To overcome the experimental variation among different research laboratories and techniques, in this review, we also critically discussed our recent complementary single-molecule conductance case studies of different anchoring groups carried out by employing STM-BJ and MCBJ setups to have a critical comparison of different anchoring groups under well-controlled conditions.[15, 17, 42, 43] On the basis of statistical analysis of conductance-distance and current-voltage traces, we have explored the evolution of single molecular junctions formed with various anchoring groups (see Fig. 1) with different binding and electron transport mechanisms (HOMO or LUMO controlled), ranging from weak interaction with the electrode surfaces to strong metal-carbon bond.[15, 17, 42-45] Qualitative and quantitative comparison of the statistically significant results provides clear understanding of the conductance variation for different junction geometries formed during the stretching process.

Break Junction Techniques

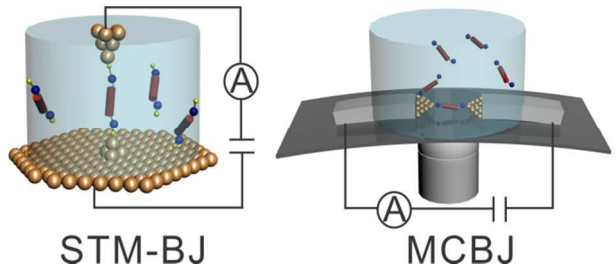

Figure 1: Schematic illustration of STM-break junction (STM-BJ) and mechanically controllable break junction (MCBJ).

Break junctions techniques are extensively used for measuring conductances in single molecular junctions. Two major types of break junctions will be described below: (1) Scanning tunneling microscopy based break junctions (STM-BJ); (2) Mechanically controllable break junctions (MCBJ). Figure.1 shows the schematic illustrations of STM-BJ and MCBJ.

Scanning tunneling microscopy- Break junction:

This technique was initially used to create metallic contacts for the study of conductance quantization of metal-metal contacts. In 2003, Xu et al.,[46] developed an STM-BJ technique, which allowed creating thousands of molecular junctions by repeatedly moving a STM tip into and out of contact with the substrate in the presence of molecules of interest.

A typical STM-based break junction experiment can be divided into following steps:[15, 17]

1. The STM tip is first controlled at a preset position using feedback control through measuring the tunneling current.
2. The STM feedback is then switched off, and the tip approaches the substrate, either modified and/or with target molecules in solution, at a constant x-y position until a preset upper limit of the current is reached (typically > 10 G_0), which leads to the formation of a metal-metal (in our experiments typically gold-gold) contacts.
3. After a short residence time, the tip is retracted from the substrate. First, the metal-metal contact breaks, and molecular junctions can be formed. Upon further pulling, the number of molecular junctions decreases upon breaking of contacts between the molecule and the metal lead. By choosing proper experimental conditions one may end up with a single molecule junction before the contacts breaks completely. During the retraction of the tip, a current-distance curve is recorded.
4. The entire cycle is repeated several thousand times to obtain a sufficient amount of data for the subsequent statistical analysis.

The advantages of the STM-BJ technique: STM allows imaging the surfaces before, during and after the transport experiment. Imaging of the bare substrate or respective modified substrate gives valuable information about the structure of the SAM and also allows positioning precisely the tip on the targeted area of the substrate. The development of tip coating techniques allows performing the STM-BJ experiments also under electrochemical potential control, which offers an extra degree of freedom to study redox active molecules for molecular electronics targets as well as for a wide range of recognition and reactivity applications.

Mechanically controllable break junction:

The MCBJ technique was developed and introduced by Moreland and Ekin in 1985.[47] They used a thin wire of a Nb-Sn filament mounted on a flexible glass beam. Using this configuration they measured electron tunneling characteristics of superconductors. Later in 1992, Muller et al.[48] coined the name mechanically controllable break junction.

The working principle of MCBJ is as follows: The MCBJ technique relies on the formation and rupture of molecular junctions between horizontally suspended gold wires. A flexible substrate is connected by two fixed beams on top and one movable beam on bottom (Fig. 1). A mechanical actuator, such as a piezo-stack transducer or a stepper motor, drives a pushing rod (moveable beam) to bend the substrate leading to an elongation and finally breaking of the metallic bridge to form a metal-metal nanogap. MCBJ sample can be prepared manually by fixing a metal wire onto flexible substrate using epoxy glue and notching the central part of the wire to create a constriction point.[13] An alternative way to create the nanobridge is based on microfabrication techniques. Accurate control of the width of the nano gap Δd, can be achieved.

MCBJ is rather insensitive to external mechanical vibration, in particularly as compared to STM-BJ for measurements at room temperature in a liquid environment. The other advantage of the MCBJ technique is that it offers an extra flexibly to be combined with other spectroscopic techniques such as simultaneous UV/VIS and/or Raman spectroscopy[49] to monitor structure information on the molecular junction simultaneously with the transport experiments. The MCBJ methodology has been also successfully implemented for measurements under cryogenic temperatures thus providing access to inelastic tunneling spectroscopy as a structure-sensitive spectroscopic approach. Furthermore, the high mechanical stability associated with MCBJ setup allows monitoring I-V curves simultaneously during the stretching and approaching processes of molecular junction elongation respective compression.[17]

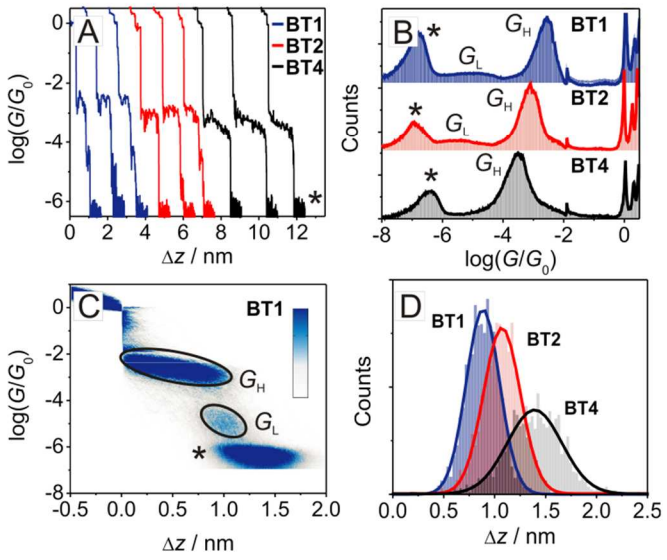

Figure 2: (A-D) Conductance measurements of BT-end-capped oligoynes in TMB/THF (4:1, v/v) employing a STM-BJ recorded with V_{bias} = 0.1 V and a stretching rate of 58 nm s^{-1}. (A) Typical conductance distance traces of BT1, BT2 and BT4. (B) 1D conductance histograms. The asterisk indicates the noise level of the set-up. The small spike at $\log(G/G_0) \approx -2$ in panel B is an artefact related to the switching of the amplifier stage. (C) 2D conductance histograms generated from 2000 individual curves and (D) Characteristic length histograms analyzed in the high conductance region (H: $0.7G_0 - 3.2 \times 10^{-4} G_0$). Reprinted with permission from ref[43]

There are also a series of developments focusing on the quantitative understanding of the data obtained from the break junction measurement. Research groups across the world used several different data selection and analysis procedures to extract the conductance values of the single molecular junctions. In this prospective, we briefly describe the most used data analysis procedures (without any data selection) to extract the single molecule junction conductance measurements.

Fig. 2A displays three typical sets of conductance $\log(G/G_0)$ versus distance (Δz) traces from the measurements with dihydrobenzo[b]thiophene-terminated oligoynes (BT1, BT2 and BT4, where 1,2 and 4 correspond to the number of -C≡C- bonds) in THF/TMB using the STM-BJ approach. Similar curves are also observed for the measurements with MCBJ technique.[43] Typical conductance histograms constructed from the analysis of these conductance-distance traces are shown in Fig. 2.

I. 1D conductance histograms: The basic strategy to build a 1D conductance histogram was communicated by Gonzalez et al.[50] The 1D conductance histograms were constructed by taking the logarithm of the entire conductance trace and binning the data using a bin size of 1000 (Fig. 2B). We do not perform any background subtraction and, typically, use 2000 traces without any data selection. The peaks in the conductance histograms were fitted with Gaussians, and from the resulting parameters the most probable conductance values were calculated.

II. 2D conductance histograms: To gain further insight into the evolution of molecular junctions during the formation, elongation and break down steps, two dimensional histograms (2D) are constructed [15, 17, 51, 52] (Fig. 2C) by aligning individual conductance traces using the "snap-back" after gold-gold contact break as reference (set $\Delta z = 0$ and $G = 0.7\ G_0$). The sharp decrease in conductance upon breaking a junction justifies this choice. Typically, we use a bin size of 1000 x 1000 ($\log(G/G_0)$ x nm) in 2D space.

Master curves were constructed by calculating the most probable conductance values from the Gaussian fits to cross sections of the 2D histogram at different displacement positions Δz. These curves give an additional information about the junction evolution as well as the standard derivations from Gaussian fits to cross-sections of the 2D histograms at different displacement positions Δz, which is a direct measure of the junction variation.

III. Characteristic length histograms: We plot all characteristic length histograms in the Δz scale (Fig. 2D). For each experimentally measured and calibrated (in distance units) current-distance trace, the number of data points in the conductance interval [high conductance limit (G_1), low conductance limit (G_2)] were linearly binned using a bin width of 0.025 nm. The most probable characteristic length of a molecular junction Δz^* was obtained by a Gaussian fit to the experimental data. In order to estimate the absolute distances between the two gold electrodes in the most probable configurations prior to breaking we need to consider the "snap-back" distance $\Delta z_{corr} = 0.5$ nm, i.e. the fast relaxation of gold electrodes upon breaking a monatomic gold-gold contact.[17, 53, 54] The most-probable absolute displacements z_H^* or z_L^* in an experimental molecular junction formed between a gold STM-tip and an Au(111) surface is obtained by adding the snap-back distance to the relative displacement Δz, i.e., $z_i^* = \Delta z_i^* + \Delta z_{corr}$, i = H, L. Moreover, by analyzing the relative displacement (Δz_i) distribution allows the quantification of the junction formation probability (JFP),[17] i.e., number of successfully formed molecular junctions out of all traces recorded. This provides information about the robustness of the anchoring binding to the electrode surface.

Aforementioned data analysis methods will help to understand the anchoring group influence on single molecular junction formation, evolution and charge transport in break junction experiments.

The role of anchoring group in single-molecule junction

Decisively, an ideal molecular anchoring group expected to provide following characteristics:

Role I: Well-defined and reproducible binding: Small conductance variation (regular binding geometry).

Role II: Sufficiently strong anchoring: Long stretching distance and sufficiently high junction formation probability.

Role III: Electronically transparent nature: Relatively high conductance (small contact resistance).

Various anchoring groups have been investigated for single molecular electronics applications, such as amino (-NH_2),[29, 55] pyridyl (-PY),[17, 31, 46, 53] thiol (-SH),[15, 56-58] isothiocyanide (-SCN),[59] cyanide (-CN),[52, 60] nitro (-NO_2),[60] carboxylic acid (-COOH), dimethyl phosphine (-PMe_2),[61] methyl sulphide (-SMe),[61] C_{60},[51, 62, 63] hydroxyl (-OH),[64] and carbodithiolate.[65] However, different anchoring groups possess different coupling strengths and contact geometries, which significantly affect the charge transport properties of the molecular junctions.

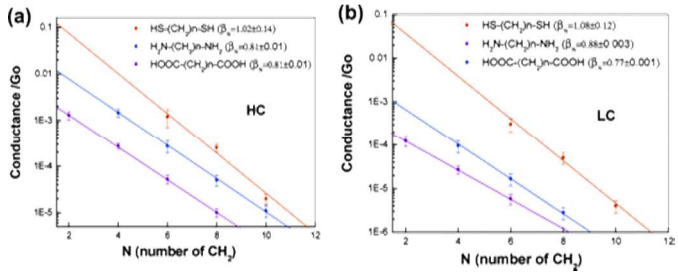

Figure 3: Logarithmic plots of single-molecule conductance vs molecular length for dithiol- (orange), diamine- (blue), and dicarboxylic-acid-terminated (purple) alkanes: (a) HC and (b) LC. Reprinted with permission from ref [33]

Tao et al.[33] systematically compared conductance of aliphatic molecular wires with –COOH, -SH and -NH_2 anchoring groups (Fig.3), which showed a conductance decrease in the following sequence: Au-SH > Au-NH_2 > Au-COOH. Authors also found that the prefactor of the exponential decay function, which reflects the contact resistance, is highly sensitive to the anchoring group, which varies in the order of Au-S > Au-NH_2 > Au-COOH, but the decay constant is weakly dependent on the anchoring group. They attributed their observations to different electronic couplings between the molecules and the electrodes and alignments of the molecular energy levels relative to the Fermi energy level of the electrodes introduced by different anchoring groups. They also obtained the binding strength information by measuring the average length over which one can stretch each molecular junction until it breaks and found that it varies in the order of Au-S > Au-NH_2 > Au-COOH. This observation is consistent with the binding strengths of three anchoring groups to gold.

Venkatraman *et. al.*[61, 66, 67] showed in a series of systematic case studies that -NH_2 forms relatively uniform molecular binding geometry (binds to the under coordinated gold atoms, which gives rather sharp conductance peaks in the histograms) compared to the isocynide anchoring group, –SH anchoring group, which exhibits strong geometry-dependent coupling, charge transport properties, i.e broad conductance features in the conductance histograms (Fig. 4).

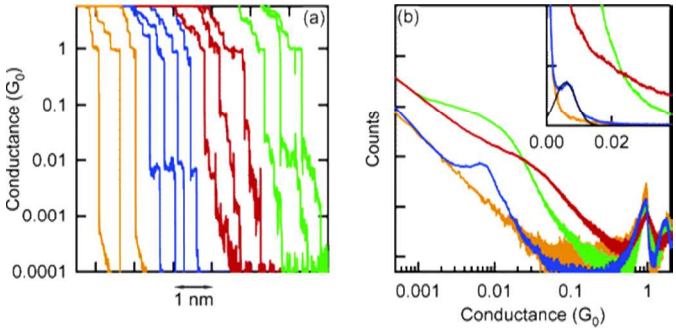

Figure 4: (a) Sample conductance traces measured without molecules (yellow) and with 1,4-benzenediamine (blue), 1,4-benzenedithiol (red), and 1,4-benzenediisonitrile (green) shown on a semilog plot. (b) Conductance histograms constructed from over 3000 traces measured in the presence of 1,4-benzenediamine (blue), 1,4-benzenedithiol (red), and 1,4-benzenediisonitrile (green), control histogram of Au without molecules is also shown (yellow) shown on a log–log plot. Histograms are normalized by the number of traces used to construct the histograms. Inset: same data on a linear plot showing a Gaussian fit to the peak (black curve). Bin size is 10^{-4} G_0. Reprinted with permission from ref[67]

Lörtscher et al.[34] studied the influence of molecule-metal coupling on transport through single-molecule junctions using thiol and isocyano anchoring groups. Characterization of the molecular junctions were done by acquiring both low-bias conductance histograms and variable-bias current–voltage characteristics. The molecular-level broadening in resonance was found to be 40 % higher for the thiol than that for the isocyano coupling. Furthermore, the quantitative single-molecule conductances at low voltages (5 mV) off-resonance were demonstrated to be 25 % smaller for the isocyano coupling, hence being in good agreement with the level broadening. Based on these experimental results, authors concluded that the isocyano groups were the better choice as linker groups under ultrahigh-vacuum conditions, because they provides higher surface mobility, indicated by less instability in the I-V curves, and a reduced line broadening, at almost identical conductance.

Tsutsui et al.[68] compared the thermodynamic stability of the two most widely studied metal-molecule systems, Au-S and Au-NH_2. Their results shown that Au-thiol bonds are far more stable than Au-amine linkages through exhibiting 2-fold longer natural lifetime of Au-aminobenzenethiol-Au single-molecule junctions compared to the Au-benzenediamine-Au counterpart. They also find that a single-molecule device composed of Au-thiol links is a factor of 100000 more stable than that configured with Au-amine contacts.

However, the results obtained by Arroyo et al.[69] have shown that the apparent stretching length L_S is determined not only by the length of the molecule, but also by the elastic and plastic deformations of the gold electrode contacts (Fig. 5). These deformations can be considerably affected by the molecules

attached to the electrodes, if their anchor groups bind strongly enough.

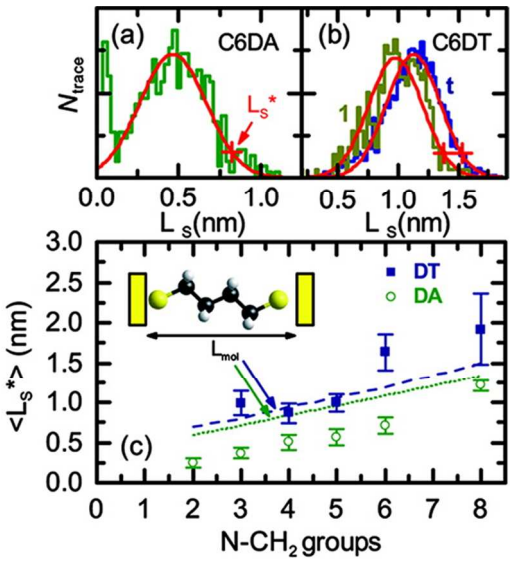

Figure 5: Apparent stretching length L_S distribution of a measurement of hexane diamine (C6DA) (a) and hexane dithiol (C6DT) (b) (t, total set of traces; 1, only traces with sharp G decay after 1 G_0). The red lines correspond to Gaussian fits to the data. LS* is the distance at which the distribution decays to 20% of its maximum (red crosses). (c) Variation of ⟨LS*⟩ with the number of carbons in the alkane. ⟨LS*⟩ is the averaged LS* over several measurements. The lines are the calculated molecular lengths L_{mol} for DT (dashed) and DA (dotted). Reprinted with permission from ref[69]

This is an important effect to be taken into account when comparing different anchoring groups. From their experimental results authors concluded that the -NH_2 produces no apparent change in electrode behavior at nanojunctions, whereas -SH has a great impact on the deformation of the electrodes. Therefore alkane-diamines produce better defined junctions, which are more suitable as a reference model.

Park et al.,[70] showed that dimethyl phosphine (-PMe_2), methyl sulphides (-SMe) and diphenylphosphine (-PPh_2) were also promising anchoring groups for obtaining single molecular junctions with well-defined conductance values, contact resistance, binding energies and junction stability sequence: -PMe_2 > -SMe > -NH_2 (Fig. 6).[61] High conductance of PMe_2 was attributed to the π-back-donation. Parameswaran et al.[71] measured the conductance of diphenylphosphine-terminated alkane-based molecules by employing the STM-BJ technique. The conductance exhibited an exponential decrease with increasing length, as expected for saturated molecules, with a tunneling decay constant of 0.98 ± 0.04 per methylene group. Measurements of junction elongation indicate strong metal-molecule binding, with a step length that increases with the number of methylene groups in the backbone. Similarly, Frei et al.[72] reported a study on simultaneous force and conductance measurements for four different chemical linker groups. Analysis of these data shown that amine (-NH_2), methylsulfide (-SMe), and diphenylphosphine (-PPh_2) linkers result in breaking a molecular junction with a most probable breaking force of about 0.6, 0.7, and 0.8 nN, respectively. On the other hand, 1,4-butanedithiol (C4SH) linkers did not show a well-defined molecular conductance signature. These junctions were analyzed directly from force traces through automated identification of force events. Authors found that C4SH junctions on average have more force events per trace than 1,4-bis(methylsulfide) butane (C4SMe). This observation supports the idea that a strong covalent S-Au bond drives more significant rearrangement of these molecular junctions.

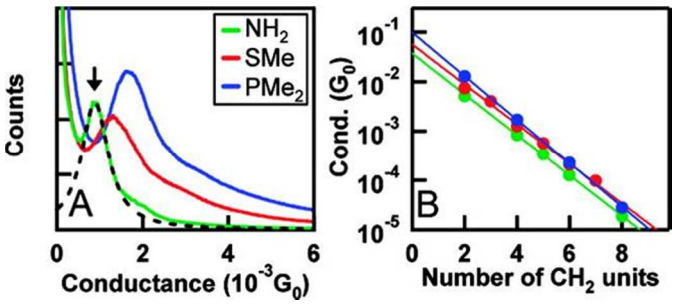

Figure 6: (A) Conductance histograms generated without data selection from over 34 000 consecutively measured traces for an *n*-butyl group terminated on each end with NH_2 (green), PMe_2 (blue), or SMe (red). (B) Conductance of all alkanes plotted against the number of methylene groups in the chain shown on a semilog scale. Reprinted with permission from ref[70]

Mishchenko et al.[52] reported a study of electron transport in single-molecule junctions formed by a series of novel biphenyl dinitriles (BPDNs). Molecular junctions formed with these chemically tailored molecules contact the gold leads through the electron-withdrawing nitrile (-C≡N) group. Their findings indicate that nitrile based metal-molecule-metal junctions represent a unique platform for the reliable construction of nanoscale molecular assemblies with very uniform electric properties.

Yokota et al.[73] demonstrated that the terthiophenediselenol (3TSe) single molecule junctions have a higher single-molecule conductance than terthiophenedithiol (3TS) (Fig. 7) and they demonstrated that replacing S atoms with Se atoms is a promising molecule-electrode bonding design for a high single-molecule conductance.

Xing et al.[65] investigated the single-molecule conductances in phenylene-ethynylene molecules terminated with thiol and carbodithioate linkers, using the STM-BJ method and a nonequilibrium Green's function approach. Their results demonstrated that the carbodithioate linker augments electronic coupling to the metal electrode and lowers the effective barrier for charge transport relative to the conventional thiol linker, thus enhancing the conductance of the linker-phenylene-ethynylene-linker unit. Borguet et al.[64] systematically studied the anchoring group effect on phorphyrin molecular junctions and showed the following conductance sequence: PY > -NH_2 > -SO_3^- > -CN > -COOH. Ie et al.[74] showed that the stability of molecular junctions can be improved by using a pyridine-based tripodal anchoring group. Li et al.[75] (junction formed with porphyrin with four identical -PY anchoring groups), Kiguchi et al.[76] (molecular junction formed with benzene dithiol (BDT)

and benzene diamine (BDA) molecules) and Venkataraman et al.[27] demonstrated a significant effect of anchoring position on the single molecule conductance.

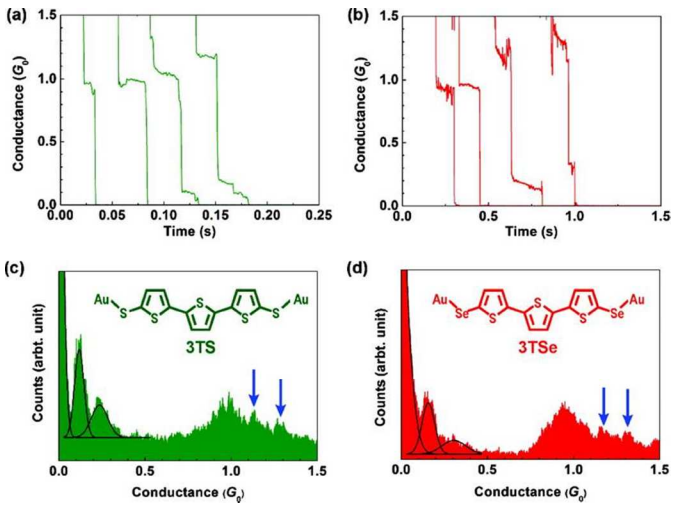

Figure 7: Typical conductance traces of (a) 3TS and (b) 3TSe junctions. Conductance histograms of (c) 3TS and (d) 3TSe junctions constructed from 1000 and 1100 conductance traces, respectively. Black lines show Gaussian fitting to peak profiles. Conductance peaks in (c) and (d) are observed at integer multiples of *G*3TS = 0.12*G*0 and *G*3TSe = 0.16*G*0, corresponding to the 3TS and 3TSe single-molecule conductance, respectively. Reprinted with permission from ref[73]

It is well known that C_{60} can hybridize strongly with gold and platinum surfaces.[77] Due to their high symmetry and their affinity to noble metals, fullerenes are very interesting candidates for anchoring. To demonstrate the C_{60} anchoring with gold surface, Martin et al.,[51] compared the low-bias conductances and junction stabilities of 1,4-bis(fullero[c]pyrrolidin-1-yl)benzene (BDC_{60}) to those of 1,4-benzenediamine (BDA) and 1,4-benzenedithiol (BDT) by using MCBJ. Results revealed that the fullerene-anchoring leads to a considerably lower spread in low-bias conductance as compared to thiols (Fig. 8). In addition, junctions of fullerene-anchored benzenes exhibit an increased stretching length before breaking.

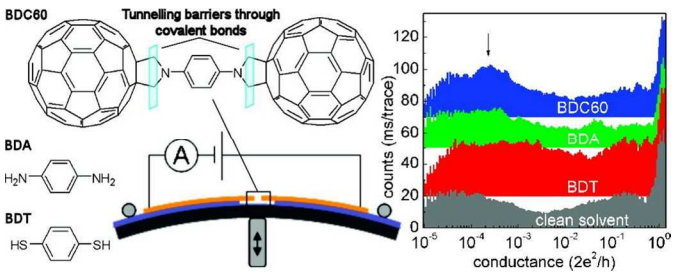

Figure 8: Molecular structures of the studied benzene derivatives, schematic of a mechanically controllable break junction, and the respective conductance histograms. Reprinted with permission from ref[51]

Recently, Kiguchi et al.,[62] reported rather high conductance values for metal-carbon coupling, such as C_{60},[51] benzene, and π-stacked benzene[78] on gold, platinum and silver electrodes.[22, 62, 79] The conductive π orbital directly hybridizes with the orbital of the metal electrodes, leading to high conductivity. Similarly, Kiguchi et al.,[80] investigated the single molecule conductance and atomic structure of single ethylene and acetylene molecule bound to Pt electrodes via di-σ and π bonds. Single molecule junctions formed with ethylene, acetylene have a conductance comparable to that of metal atomic junctions (around $0.9G_0$: $G_0 = 2e^2/h$) due to effective hybridization between metal and the π molecular orbital. By using the highly conductive single molecule junctions, authors investigated the characteristics of vibration spectroscopy of the single molecule junction in an intermediate regime between tunneling and contact. The vibration modes that could modify the conduction orbital were excited for the ethylene and acetylene molecule junctions. The crossover between conductance enhancement and suppression was observed for the single ethylene molecule junction, whereas clear crossover was not observed for the acetylene molecule junction, reflecting the number of conduction orbitals in the single molecule junction.

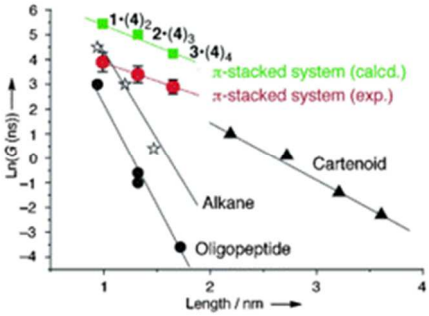

Figure 9: Distance dependence of observed conductance G for single π -stacked junctions 1·(4)2, 2·(4)3, and 3·(4)4. Typical single-molecule conductances for saturated (alkane chains and peptides) and conjugated (carotenoids) organic molecules are also shown. Reprinted with permission from reference[82, 83]

Schneebeli et al.[78] employed the STM-BJ technique to measure the single-molecule conductance of multiple π-π-stacked aromatic rings (up to four stacked benzene rings held together in an eclipsed fashion via a paracyclophane scaffold). Authors found that the strained hydrocarbons can couple directly to gold electrodes during the measurements. Hence, they did not require any heteroatom binding groups as electrical contacts. The experimental results showed an exponential decay of the conductance with an increasing number of stacked benzene rings, indicating a nonresonant tunneling mechanism. Similarly, Kiguchi et al.[22, 81-83] reported a systematic study on electron transport through single molecules comprising of aromatic stacks enclosed in self-assembled cages. Authors demonstrated with their experimental results, that they were able to precisely calibrate the electron-transport distance and single-molecule π stacks exhibit good conductance with only a moderate loss of conductance with increasing transport length (Fig. 9). These experimental results further showed that the molecular junctions can form without anchoring groups like thiol, thus potentially simplifying the synthesis of organic molecular wires and adding a new method for measuring the conductance of complex single-molecule molecular junctions.

Although π-stacked molecular junctions are quite attractive, however, their junction stability is relatively low due to weak interactions with the electrode surface. To overcome the junction stability problem, Venkatraman et al.[84] and Hong et al.,[44] demonstrated the formation of direct Au-C bonded single molecular junctions for alkanes and π-conjugated aromatic or alkane molecules upon spontaneous cleavage of trimethyl tin or trimethyl silane end group. These covalent Au-C bonded single molecular junctions led to conductances up to 100 times larger compared to analogous $–NH_2$ or –SH -terminated alkane/aromatic molecules. Similarly, Tao et al.[35] demonstrated the in-situ formation of Au-C bond in single-molecule junctions by means of electrochemically reducing two axial diazonium terminal groups on a molecule. Authors reported enhancement in the yield of molecular junction formation as the electrochemical potential of both junction electrodes approach the reduction potential of the diazonium terminal groups. Step length analysis showed that the molecular junction is significantly more stable, and can be pulled over a longer distance than a comparable junction created with amine anchoring bonds. The stability of the junction is explained by the calculated lower binding energy associated with the direct Au–C bond compared with the Au–N bond.

The length dependence of molecular conductance is also strongly affected by anchoring groups. Hines et al.,[36] reported a transition between tunneling and hopping mechanism in single-molecule junctions formed with four molecular wires (with thiol anchoring group) ranging from 3.1 to 9.4 nm in length. The two shortest wires displayed strongly length-dependent and temperature-invariant conductance behavior, whereas two longer wires showed weakly length dependent and temperature variant behavior. This trend is consistent with the model where by conduction occurs by two different mechanisms in the family of wires (tunneling and hopping). Similarly, based on STM-BJ and conducting probe atomic force microscopy (CP-AFM) investigations on amine-terminated OPE molecules (with molecular lengths ranging from 0.98 nm to 5.11 nm), Wang et al.[37] reported the transition of the transport mechanism from tunneling to hopping. Followed by this work, the same group showed that the incorporation of ferrocene into the OPE backbone, leads to an enhanced conductance in tunneling and hopping regimes.[85] For long-range charge transport in a molecular system it is very important that the decay constant β is low and that means there is a strong electronic coupling between the molecule bridge and the terminal contacts. To demonstrate this effect, Sedghi and co-workers synthesized a series of porphyrin oligomers with thiol anchoring group.[86] They measured the conductance of these molecule by employing I(t) and I(s) method and found a very low decay constant, $\beta = (0.04 \pm 0.006)$ $Å^{-1}$, which is considerably lower than the values generally observed for π-conjugated organic bridges (β values in the range 0.1~0.6 $Å^{-1}$). Li et al. observed similar results with meso-to-meso ethyne-bridged (porphinato)zinc(II) structures connected to gold electrodes via (4-thiophenyl)ethynyl termini and determined $\beta = 0.034$ $Å^{-1}$.[87] Kolivoska et al.[88] reported a study on a series of extended viologen molecules with thiol anchoring groups, which showed even smaller attenuation factor ($\beta = 0.006 \pm 0.0004$ $Å^{-1}$), measured by using STM-BJ technique. Lötscher et al. [89] measured the conductance of a series of oligophenylene rods (with thiol anchors) of increasing lengths. A linear increase of the conductance gap with increasing number of phenyl rings (from 260 meV for one ring to 580 meV for four rings) was revealed. The authors also demonstrated that the conductance did not primarily depend on the molecular length, but was rather limited by the injection of the charge carriers at the metal molecule interface, which signified the importance of the anchoring group in metal-molecule-metal junctions.

Systematic comparison of anchoring group effect on the junction evolution and conductance of oligoyne and Oligo(phenylene ethenylene) (OPE) type molecular junctions

Most of the aforementioned experimental studies were focused mainly on the search for new anchoring groups and their effect on the molecular conductance. However, a clear understanding of junction evolution during junction formation and breaking (stretching process) was still missing. To get some insight on how anchoring group affects charge transport through a molecular junction, junction evolution and structure-property relationship, we systematically compared and critically discussed the results from our previous case studies (Fig. 9).

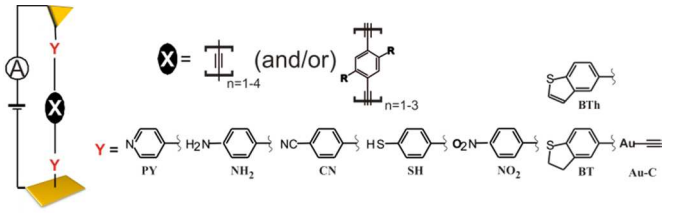

Figure 9: Schematic illustration of a molecular junction, (where "X" represents the central core of the molecule, "Y" represents the anchoring group) and the structures of the anchoring groups investigated.

I. Conductance decay and variation with displacement (Role.I):
The anchoring group determine the binding geometry, which significantly influence the junction evolution behavior and stability. In an attempt to understand the evolution of the molecular conductance upon stretching, we calculated the most probable conductance values (G^{st}) as well as the standard derivations from Gaussian fits to cross-sections of the 2D histograms at different displacement positions Δz.[17, 43]
Figure 10 displays the distributions of conductance-variation histograms obtained by decomposing the 2D histograms (such as in Figure 2C) into 1D histograms at different relative displacements Δz and subsequent Gaussian fits.[44] The resulting width of the distributions varies depending on the anchoring group. The conductance variation determined from the peak in the distributions increase according to the following sequence: PY < BT < NH_2<Au-C < SH < CN<NO_2 for tolane (oligoyne n = 1).[17, 43, 44] This trend can be attributed to (i) the uniformity of the binding geometries and (ii) a decrease in binding energy

and/or junction stability (CN anchoring group). The conductance variation increases also with the molecular length within each family, which is particularly attributed to the decrease in junction stability and less uniform molecular junctions.[43]

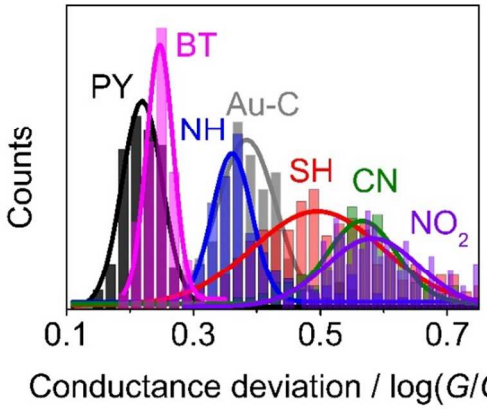

Figure. 10: Conductance variation distributions in the high conductance range, for tolane with different anchoring groups. Data taken from ref[50,51]

II. Junction formation probability (Role. II):

For molecular junctions formed by BT-terminated oligoyne derivatives no direct tunneling traces through the solution were observed, indicating that the junction formation probability approaches 100%. Comparison of different anchoring group junction formation probabilities reveals the following trend: BTh < NO_2 < CN < NH_2 < Au-C < SH ≈ PY ≈ BT.[17, 43, 44, 90] This sequence represents the indirect measure of the stability of the molecular junctions, and indicates that molecular junctions formed with CN, BTh and NO_2–caped oligoyne / OPE molecules are rather unstable and break at an inclined angle with respect to the surface normal before they are fully extended.[90] However, we note that the results of the current study deviate from recent observations of Zotti et al.,[60] who concluded that NO_2-terminated tolanes form rather stable molecular junctions under ambient conditions with MCBJ. This difference may arise from the nature of the different experimental conditions in both studies.[60, 90]

III. Conductance and length dependence of single molecule tolane /oligoyne/oligophenyleneethynylene junctions (Role. III):

The electronic coupling of the molecular junction and the electrode show great dependence on the different anchoring group. To demonstrate the correlation between anchoring group and length dependence of single-molecule conductance, we investigated the influence of molecular length on junction conductance and stability of the oligoyne-type molecular junctions (n = 1, 2, 4 with BT, PY, SH, NH_2, CN, NO_2 and BTh anchoring groups) and OPE-type molecular junctions (n = 1, 2, 3 with SH, PY, Au-C anchoring groups) following the strategy described above for BT-terminated derivatives.[43]

Figure 11 displays the dependencies of the most probable conductances of oligoynes (Figure 11A) and OPE's (Figure 11B) versus the molecular length (L).[15, 44, 45] The analysis of the most probable high (H) conductance values G_H* reveals an exponential dependence on the distance for oligoynes-type and OPE-type molecular wires with different anchoring groups according to $G_H^* = G_C \cdot \exp(-\beta_H \cdot L)$. $G_C = 1/R_C$ represents an effective contact conductance reflecting the electronic coupling at the molecule-electrode interface. β_H is the attenuation constant, which characterizes the electronic coupling in a specific molecular backbone in function of its length. The experimentally determined β_H values range from (1.7±0.1) nm^{-1} (CN) to (5.4±0.3) nm^{-1} (NO_2) for oligoynes-type molecular rods, and for OPE type molecular wires with SH,[15] PY,[45] Au-C[44] anchoring groups attenuation constant value is β_H = (3.3 ± 0.1) nm^{-1}. Following trend is tentatively observed for the oligoyne-type molecular rods: β_H(CN) < β_H(BTh) ≈ β_H(NH_2) < β_H(BT) ≈ β_H(PY) < β_H(SH) < β_H(NO_2).[43, 90] Due to limited stability and unavailability of experimental conductance data for SH-, NH_2-capped oligoyne with n = 4, attenuation factor values for NH_2, SH family should be considered with caution. The distinctly different values of β_H demonstrate that the nature of the anchor group controls the strength of the electronic coupling to the metal leads, the position of the energy levels involved in the electron transport across the single molecule junction as well as their coupling into the molecular wire backbone.

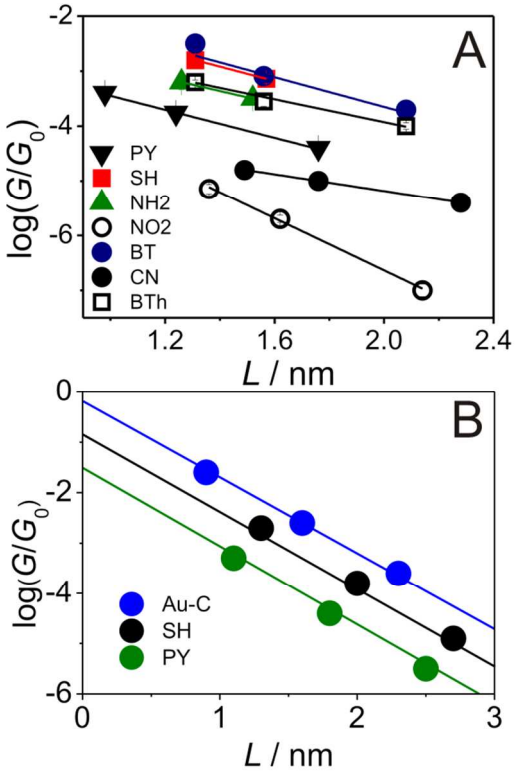

Figure 11: (A) Most probable single junction conductance values of the seven families of oligoynes as determined from the analysis of 1D and 2D conductance histograms verses molecular length *L*. Reprinted with permission from ref[42] (B) Most probable single junction conductance values of the three families of Oligophenyleneethynylene (OPE) as determined from the analysis of 1D and 2D conductance histograms verses molecular length *L*. Data taken from ref[42]

The experimental values of the decay parameter β for different molecular bridges are reported in literature as follows: saturated alkanes[56, 91, 92] (7 - 11 nm^{-1}) > oligophenyls[93, 94] (OP, 3.5 - 5 nm^{-1}) > oligo(phenylene-ethynylenes)[15, 37, 95, 96] (OPEs, 2.0 - 3.4 nm^{-1}) > oligophenyleimine[38] (OPI, 3 nm^{-1}) > carotenoid polyenes[97, 98] (1.7 - 2.2 nm^{-1}) > oligo(phenylene-vinylenes)[91, 99] (OPVs, 1.7 - 1.8 nm^{-1}) > benzene-furan oligoaryls[99] (1.1 - 1.3 nm^{-1}) > oligothiophenes[100] (OT, 1.0 nm^{-1}) > carbodithioate-capped OPEs[95] (CT, 0.5 nm^{-1}) > porphyrin oligomers[86] (0.4 nm^{-1}) > pyridyl-capped oligoynes[101] (0.6 nm^{-1}). Attenuation constant values β_H obtained in our studies are in the same range as those of typical conjugated wires, such as OPEs, OPVs and OPIs. We also observed that the effective contact resistances $R_C = 1/G_C$, determined by extrapolating the G_H* versus L dependencies towards 0, leads to the following sequence for (i) oligoynes with different anchoring groups:[43, 90] $R_C(BT) < R_C(SH) < R_C(NH_2) < R_C(PY) < R_C(NO_2) \approx R_C(BTh) << R_C(CN)$ and (ii) OPE's with different anchoring groups: R_C(Au-C) < $R_C(SH) < R_C(PY)$.[15, 45, 90] The contact resistance of OPE with Au-C covalent contact is of the order of a metallic Au-Au nanocontacts indicating an excellent electronic coupling of the Au-C coupling unit with the electrode. The similar trends for both molecular systems demonstrate that the contact resistance values are highly dependent on the anchoring group. It is also suggested that contribution from the anchoring group must be considered to get the electronically transparent coupling between the molecular backbone and the electrodes.

Summary and outlook

We have summarized systematic investigations on effect of anchoring group on single molecule conductance of several families of oligoyne/ oligo(phenyleneethynylene), alkane and other-type molecular junctions (BT, PY, SH, NH_2, CN, NO_2, BTh, SMe, PPh2, NC, SeH, C60, stacked systems) -focusing on two complementary techniques, namely scanning tunnelling microscopy break junction (STM-BJ) and mechanically controlled break junction techniques (MCBJ) based on the some of the important studies published in literature and the case studies from our own work.

To design a molecular system for molecular electronics applications, one must take following aspects into account: The electronic coupling of the molecular junction and the electrode show great dependence on the different anchoring group. Thus anchoring are expected to provide well-defined and reproducible binding, sufficiently strong anchoring and electronically transparent nature. Based on a systematical comparison within our lab and the results published in literature, it is suggested that BT anchoring group and Au-C are promising anchoring groups for the future molecular electronics applications.

Acknowledgements

We thank Prof. Silvio Decurtins, Prof. Martin Bryce, Prof. Jan. C Hummelen and Prof. Colin Lambert for their fruitful collaborations. We acknowledge the funding support by the Swiss National Science Foundation (Grant No. 200020-144471), EPSRC and by EC FP7 ITN "MOLESCO". A.R. acknowledges FP7 project ACMOL (No 618082).

Notes and references

[a] Department of Chemistry and Biochemistry, University of Bern, Freiestrasse 3, CH-3012, Bern, Switzerland.
E-mail: bhadra.chemistry@gmail.com; hong@dcb.unibe.ch

1. A. Aviram and M. Ratner, *Chem. Phys. Lett.*, 1974, **29**, 277-283.
2. E. Robert M. Metzger, *"Unimolecular Electronics" in Topics in Current Chemistry*, Springer Verlag: Berlin, **2012**.
3. H. B. Akkerman and B. de Boer, *J. Phys. Condens. Matter.*, 2008, **20**, 013001.
4. N. J. Tao, *Nat. Nanotechnol.*, 2006, **1**, 173-181.
5. D. Xiang, H. Jeong, T. Lee and D. Mayer, *Adv. Mater.*, 2013, **25**, 4845-4867.
6. R. L. McCreery and A. J. Bergren, *Adv. Mater.*, 2009, **21**, 4303-4322.
7. N. Tuccitto, V. Ferri, M. Cavazzini, S. Quici, G. Zhavnerko, A. Licciardello and M. A. Rampi, *Nat. Mater.*, 2009, **8**, 41-46.
8. R. C. Chiechi, E. A. Weiss, M. D. Dickey and G. M. Whitesides, *Angew. Chem. Int. Ed.*, 2008, **47**, 142-144.
9. J. G. Kushmerick, D. B. Holt, S. K. Pollack, M. A. Ratner, J. C. Yang, T. L. Schull, J. Naciri, M. H. Moore and R. Shashidhar, *J. Am. Chem. Soc.*, 2002, **124**, 10654-10655.
10. J. Chen, M. A. Reed, A. M. Rawlett and J. M. Tour, *Science*, 1999, **286**, 1550-1552.
11. J. Liao, L. Bernard, M. Langer, C. Schonenberger and M. Calame, *Adv. Mater.*, 2006, **18**, 2444-2447.
12. Z. J. Donhauser, B. A. Mantooth, K. F. Kelly, L. A. Bumm, J. D. Monnell, J. J. Stapleton, D. W. Price, A. M. Rawlett, D. L. Allara, J. M. Tour and P. S. Weiss, *Science*, 2001, **292**, 2303-2307.
13. W. Hong, H. Valkenier, G. Meszaros, D. Z. Manrique, A. Mishchenko, A. Putz, P. M. Garcia, C. J. Lambert, J. C. Hummelen and T. Wandlowski, *Beilstein J. Nanotechnol.*, 2011, **2**, 699-713.
14. B. Q. Xu and N. J. Tao, *Science*, 2003, **301**, 1221-1223.
15. V. Kaliginedi, P. Moreno-García, H. Valkenier, W. Hong, V. M. García-Suárez, P. Buiter, J. L. H. Otten, J. C. Hummelen, C. J. Lambert and T. Wandlowski, *J. Am. Chem. Soc.*, 2012, **134**, 5262-5275.
16. M. F. M. Frei, S. V. Aradhya, M. Koentopp, M. S. Hybertsen and L. Venkataraman, *Nano Lett.*, 2011, **11**, 1518-1523.
17. W. Hong, D. Z. Manrique, P. Moreno-García, M. Gulcur, A. Mishchenko, C. J. Lambert, M. R. Bryce and T. Wandlowski, *J. Am. Chem. Soc.*, 2012, **134**, 2292-2304.
18. I. V. Pobelov, G. Meszaros, K. Yoshida, A. Mishchenko, M. Gulcur, M. R. Bryce and T. Wandlowski, *J. Phys. Condens. Matter.*, 2012, **24**.
19. W. Haiss, R. J. Nichols, H. van Zalinge, S. J. Higgins, D. Bethell and D. J. Schiffrin, *Phys. Chem. Chem. Phys.*, 2004, **6**, 4330.
20. R. J. Nichols, W. Haiss, S. J. Higgins, E. Leary, S. Martin and D. Bethell, *Phys. Chem. Chem. Phys.*, 2010, **12**, 2801.
21. H. Valkenier, C. M. Guedon, T. Markussen, K. S. Thygesen, S. J. van der Molen and J. C. Hummelen, *Phys. Chem. Chem. Phys.*, 2014, **16**, 653-662.
22. M. Kiguchi and S. Kaneko, *Phys. Chem. Chem. Phys.*, 2013, **15**, 2253-2267.

23. R. L. McCreery, H. Yan and A. J. Bergren, *Phys. Chem. Chem. Phys.*, 2013, **15**, 1065-1081.
24. B. Capozzi, Q. Chen, P. Darancet, M. Kotiuga, M. Buzzeo, J. B. Neaton, C. Nuckolls and L. Venkataraman, *Nano Lett.*, 2014, **14**, 1400-1404.
25. B. Capozzi, E. J. Dell, T. C. Berkelbach, D. R. Reichman, L. Venkataraman and L. M. Campos, *J. Am. Chem. Soc.*, 2014, **136**, 10486-10492.
26. T. Kim, Z.-F. Liu, C. Lee, J. B. Neaton and L. Venkataraman, *Proc. Natl. Acad. Sci.*, 2014, **111**, 10928-10932.
27. J. R. Quinn, F. W. Foss, L. Venkataraman, M. S. Hybertsen and R. Breslow, *J. Am. Chem. Soc.*, 2007, **129**, 6714-6715.
28. T. A. Su, J. R. Widawsky, H. Li, R. S. Klausen, J. L. Leighton, M. L. Steigerwald, L. Venkataraman and C. Nuckolls, *J. Am. Chem. Soc.*, 2013, **135**, 18331-18334.
29. L. Venkataraman, J. E. Klare, C. Nuckolls, M. S. Hybertsen and M. L. Steigerwald, *Nature*, 2006, **442**, 904-907.
30. J. Xia, B. Capozzi, S. Wei, M. Strange, A. Batra, J. R. Moreno, R. J. Amir, E. Amir, G. C. Solomon, L. Venkataraman and L. M. Campos, *Nano Lett.*, 2014, **14**, 2941-2945.
31. D. Roldan, V. Kaliginedi, S. Cobo, V. Kolivoska, C. Bucher, W. Hong, G. Royal and T. Wandlowski, *J. Am. Chem. Soc.*, 2013, **135**, 5974-5977.
32. F. Chen and N. J. Tao, *Acc. Chem. Res.*, 2009, **42**, 429-438.
33. F. Chen, X. Li, J. Hihath, Z. Huang and N. Tao, *J. Am. Chem. Soc.*, 2006, **128**, 15874-15881.
34. E. Lörtscher, C. J. Cho, M. Mayor, M. Tschudy, C. Rettner and H. Riel, *ChemPhysChem*, 2011, **12**, 1677-1682.
35. T. Hines, I. Diez-Perez, H. Nakamura, T. Shimazaki, Y. Asai and N. Tao, *J. Am. Chem. Soc.*, 2013, **135**, 3319-3322.
36. T. Hines, I. Diez-Perez, J. Hihath, H. Liu, Z.-S. Wang, J. Zhao, G. Zhou, K. Müllen and N. Tao, *J. Am. Chem. Soc.*, 2010, **132**, 11658-11664.
37. Q. Lu, K. Liu, H. M. Zhang, Z. B. Du, X. H. Wang and F. S. Wang, *ACS Nano*, 2009, **3**, 3861-3868.
38. S. H. Choi, B. Kim and C. D. Frisbie, *Science*, 2008, **320**, 1482-1486.
39. C. R. Arroyo, S. Tarkuc, R. Frisenda, J. S. Seldenthuis, C. H. M. Woerde, R. Eelkema, F. C. Grozema and H. S. J. van der Zant, *Angew. Chem. Int. Ed.*, 2013, **52**, 3152-3155.
40. C. R. Arroyo, R. Frisenda, K. Moth-Poulsen, J. S. Seldenthuis, T. Bjornholm and H. S. J. van der Zant, *Nanoscale Res. Lett.*, 2013, **8**, 1-6.
41. N. Darwish, I. Diez-Perez, S. Guo, N. Tao, J. J. Gooding and M. N. Paddon-Row, *J. Phys. Chem. C*, 2012, **116**, 21093-21097.
42. M. Gulcur, P. Moreno-Garcia, X. Zhao, M. Baghernejad, A. S. Batsanov, W. Hong, M. R. Bryce and T. Wandlowski, *Chem. Eur. J.*, 2014, **20**, 4653-4660.
43. P. Moreno-Garcia, M. Gulcur, D. Z. Manrique, T. Pope, W. Hong, V. Kaliginedi, C. Huang, A. S. Batsanov, M. R. Bryce, C. Lambert and T. Wandlowski, *J. Am. Chem. Soc.*, 2013, **135**, 12228-12240.
44. W. Hong, H. Li, S.-X. Liu, Y. Fu, J. Li, V. Kaliginedi, S. Decurtins and T. Wandlowski, *J. Am. Chem. Soc.*, 2012, **134**, 19425-19431.
45. X. Zhao, C. Huang, M. Gulcur, A. S. Batsanov, M. Baghernejad, W. Hong, M. R. Bryce and T. Wandlowski, *Chem. Mater.*, 2013, **25**, 4340-4347.
46. B. Xu and N. J. Tao, *Science*, 2003, **301**, 1221-1223.
47. J. Moreland and J. W. Ekin, *J. Appl. Phys.*, 1985, **58**, 3888.
48. C. J. Muller, J. M. van Ruitenbeek and L. J. de Jongh, *Physica C*, 1992, **191**, 485-504.
49. Z. Liu, S.-Y. Ding, Z.-B. Chen, X. Wang, J.-H. Tian, J. R. Anema, X.-S. Zhou, D.-Y. Wu, B.-W. Mao, X. Xu, B. Ren and Z.-Q. Tian, *Nat. Commun.*, 2011, **2**, 305.
50. M. T. Gonzalez, S. Wu, R. Huber, S. J. van der Molen, C. Schoenenberger and M. Calame, *Nano Lett.*, 2006, **6**, 2238-2242.
51. C. A. Martin, D. Ding, J. K. Sørensen, T. Bjørnholm, J. M. van Ruitenbeek and H. S. J. van der Zant, *J. Am. Chem. Soc.*, 2008, **130**, 13198-13199.
52. A. Mishchenko, L. A. Zotti, D. Vonlanthen, M. Burkle, F. Pauly, J. C. Cuevas, M. Mayor and T. Wandlowski, *J. Am. Chem. Soc.*, 2011, **133**, 184-187.
53. S. Y. Quek, M. Kamenetska, M. L. Steigerwald, H. J. Choi, S. G. Louie, M. S. Hybertsen, J. B. Neaton and L. Venkataraman, *Nat. Nanotechnol.*, 2009, **4**, 230-234.
54. N. Agraït, *Phys. Rep.*, 2003, **377**, 81-279.
55. M. S. Hybertsen, L. Venkataraman, J. E. Klare, A. C. Whalley, M. L. Steigerwald and C. Nuckolls, *J. Phys. Condens. Matter.*, 2008, **20**, 374115.
56. C. Li, I. Pobelov, T. Wandlowski, A. Bagrets, A. Arnold and F. Evers, *J. Am. Chem. Soc.*, 2008, **130**, 318-326.
57. A. Mishchenko, D. Vonlanthen, V. Meded, M. Bürkle, C. Li, I. V. Pobelov, A. Bagrets, J. K. Viljas, F. Pauly, F. Evers, M. Mayor and T. Wandlowski, *Nano Lett.*, 2010, **10**, 156-163.
58. F. Chen, X. Li, J. Hihath, Z. Huang and N. Tao, *J. Am. Chem. Soc.*, 2006, **128**, 15874-15881.
59. C. H. Ko, M. J. Huang, M. D. Fu and C. H. Chen, *J. Am. Chem. Soc.*, 2010, **132**, 756-764.
60. L. A. Zotti, T. Kirchner, J. C. Cuevas, F. Pauly, T. Huhn, E. Scheer and A. Erbe, *Small*, 2010, **6**, 1529-1535.
61. Y. S. Park, A. C. Whalley, M. Kamenetska, M. L. Steigerwald, M. S. Hybertsen, C. Nuckolls and L. Venkataraman, *J. Am. Chem. Soc.*, 2007, **129**, 15768-15769.
62. M. Kiguchi, *Appl. Phys. Lett.*, 2009, **95**, 073301.
63. J. Fock, J. K. Sorensen, E. Loertscher, T. Vosch, C. A. Martin, H. Riel, K. Kilsa, T. Bjornholm and H. van der Zant, *Phys. Chem. Chem. Phys.*, 2011, **13**, 14325-14332.
64. Z. Li, M. Smeu, M. A. Ratner and E. Borguet, *J. Phys. Chem. C*, 2013, **117**, 14890-14898.
65. Y. Xing, T.-H. Park, R. Venkatramani, S. Keinan, D. N. Beratan, M. J. Therien and E. Borguet, *J. Am. Chem. Soc.*, 2010, **132**, 7946-7956.
66. S. Y. Quek, L. Venkataraman, H. J. Choi, S. G. Louie, M. S. Hybertsen and J. B. Neaton, *Nano Lett.*, 2007, **7**, 3477-3482.
67. J. Ulrich, D. Esrail, W. Pontius, L. Venkataraman, D. Millar and L. H. Doerrer, *J. Phys. Chem. B*, 2006, **110**, 2462-2466.
68. M. Tsutsui, M. Taniguchi and T. Kawai, *J. Am. Chem. Soc.*, 2009, **131**, 10552-10556.
69. C. R. Arroyo, E. Leary, A. s. Castellanos-Gómez, G. Rubio-Bollinger, M. T. González and N. s. Agraït, *J. Am. Chem. Soc.*, 2011, **133**, 14313-14319.
70. Y. S. Park, A. C. Whalley, M. Kamenetska, M. L. Steigerwald, M. S. Hybertsen, C. Nuckolls and L. Venkataraman, *J. Am. Chem. Soc.*, 2007, **129**, 15768-15769.

71. R. Parameswaran, J. R. Widawsky, H. Vázquez, Y. S. Park, B. M. Boardman, C. Nuckolls, M. L. Steigerwald, M. S. Hybertsen and L. Venkataraman, *J. Phys. Chem. Lett.*, 2010, **1**, 2114-2119.
72. M. Frei, S. V. Aradhya, M. S. Hybertsen and L. Venkataraman, *J. Am. Chem. Soc.*, 2012, **134**, 4003-4006.
73. K. Yokota, M. Taniguchi, M. Tsutsui and T. Kawai, *J. Am. Chem. Soc.*, 2010, **132**, 17364-17365.
74. Y. Ie, T. Hirose, H. Nakamura, M. Kiguchi, N. Takagi, M. Kawai and Y. Aso, *J. Am. Chem. Soc.*, 2011, **133**, 3014-3022.
75. Z. Li and E. Borguet, *J. Am. Chem. Soc.*, 2012, **134**, 63-66.
76. M. Kiguchi, H. Nakamura, Y. Takahashi, T. Takahashi and T. Ohto, *J. Phys. Chem. C*, 2010, **114**, 22254-22261.
77. C. Rogero, J. I. Pascual, J. Gómez-Herrero and A. M. Baró, *The Journal of Chemical Physics*, 2002, **116**, 832.
78. S. T. Schneebeli, M. Kamenetska, Z. Cheng, R. Skouta, R. A. Friesner, L. Venkataraman and R. Breslow, *J. Am. Chem. Soc.*, 2011, **133**, 2136-2139.
79. M. Kiguchi, O. Tal, S. Wohlthat, F. Pauly, M. Krieger, D. Djukic, J. Cuevas and J. van Ruitenbeek, *Phys. Rev. Lett.*, 2008, **101**.
80. T. Nakazumi, S. Kaneko, R. Matsushita and M. Kiguchi, *J. Phys. Chem. C*, 2012, **116**, 18250-18255.
81. M. Kiguchi, J. Inatomi, Y. Takahashi, R. Tanaka, T. Osuga, T. Murase, M. Fujita, T. Tada and S. Watanabe, *Angew. Chem. Int. Ed.*, 2013, **52**, 6202-6205.
82. M. Kiguchi and S. Kaneko, *ChemPhysChem*, 2012, **13**, 1116-1126.
83. M. Kiguchi, T. Takahashi, Y. Takahashi, Y. Yamauchi, T. Murase, M. Fujita, T. Tada and S. Watanabe, *Angew. Chem. Int. Ed.*, 2011, **50**, 5707-5710.
84. Z. Liu, S.-Y. Ding, Z.-B. Chen, X. Wang, J.-H. Tian, J. R. Anema, X.-S. Zhou, D.-Y. Wu, B.-W. Mao, X. Xu, B. Ren and Z.-Q. Tian, *Nat. Commun.*, 2011, **2**, 305.
85. Q. Lu, C. Yao, X. Wang and F. Wang, *J. Phys. Chem. C*, 2012, **116**, 17853-17861.
86. G. Sedghi, K. Sawada, L. J. Esdaile, M. Hoffmann, H. L. Anderson, D. Bethell, W. Haiss, S. J. Higgins and R. J. Nichols, *J. Am. Chem. Soc.*, 2008, **130**, 8582-8583.
87. Z. Li, T.-H. Park, J. Rawson, M. J. Therien and E. Borguet, *Nano Lett.*, 2012, **12**, 2722-2727.
88. V. Kolivoska, M. Valasek, M. Gal, R. Sokolova, J. Bulickova, L. Pospisil, G. Meszaros and M. Hromadova, *J. Phys. Chem. Lett.*, 2013, **4**, 589-595.
89. E. Lörtscher, M. Elbing, M. Tschudy, C. von Hänisch, H. B. Weber, M. Mayor and H. Riel, *ChemPhysChem*, 2008, **9**, 2252-2258.
90. M. Gulcur, P. Moreno-Garcia, X. Zhao, M. Baghernejad, A. S. Batsanov, W. Hong, M. R. Bryce and T. Wandlowski, *Chem. Eur. J.*, 2014, **20**, 4653-4660.
91. H. M. Liu, N. Wang, J. W. Zhao, Y. Guo, X. Yin, F. Y. C. Boey and H. Zhang, *ChemPhysChem*, 2008, **9**, 1416-1424.
92. B. Q. Xu and N. J. J. Tao, *Science*, 2003, **301**, 1221-1223.
93. D. J. Wold, R. Haag, M. A. Rampi and C. D. Frisbie, *J. Phys. Chem. B*, 2002, **106**, 2813-2816.
94. T. Ishida, W. Mizutani, Y. Aya, H. Ogiso, S. Sasaki and H. Tokumoto, *J. Phys. Chem. B*, 2002, **106**, 5886-5892.
95. Y. J. Xing, T. H. Park, R. Venkatramani, S. Keinan, D. N. Beratan, M. J. Therien and E. Borguet, *J. Am. Chem. Soc.*, 2010, **132**, 7946-7956.
96. K. Liu, G. R. Li, X. H. Wang and F. S. Wang, *J. Phys. Chem. C*, 2008, **112**, 4342-4349.
97. J. He, F. Chen, J. Li, O. F. Sankey, Y. Terazono, C. Herrero, D. Gust, T. A. Moore, A. L. Moore and S. M. Lindsay, *J. Am. Chem. Soc.*, 2005, **127**, 1384-1385.
98. I. Visoly-Fisher, K. Daie, Y. Terazono, C. Herrero, F. Fungo, L. Otero, E. Durantini, J. J. Silber, L. Sereno, D. Gust, T. A. Moore, A. L. Moore and S. M. Lindsay, *Proc. Natl. Acad. Sci.*, 2006, **103**, 8686-8690.
99. I. W. P. Chen, M.-D. Fu, W.-H. Tseng, C.-h. Chen, C.-M. Chou and T.-Y. Luh, *Chem. Commun.*, 2007, 3074-3076.
100. R. Yamada, H. Kumazawa, T. Noutoshi, S. Tanaka and H. Tada, *Nano Lett.*, 2008, **8**, 1237-1240.
101. C. S. Wang, A. S. Batsanov, M. R. Bryce, S. Martin, R. J. Nichols, S. J. Higgins, V. M. Garcia-Suarez and C. J. Lambert, *J. Am. Chem. Soc.*, 2009, **131**, 15647-15654.

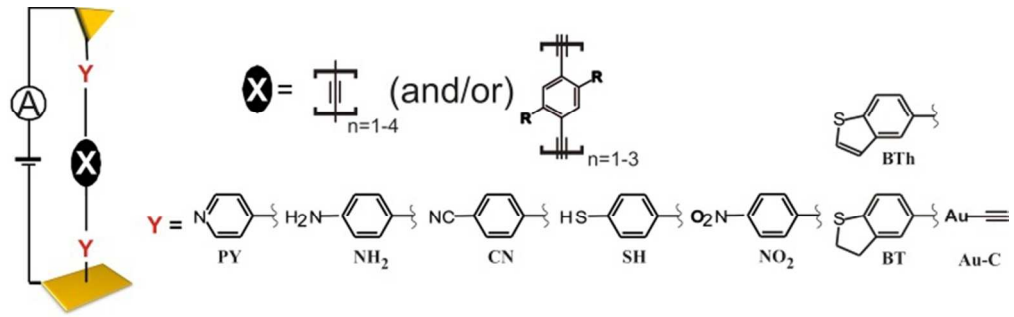

161x50mm (120 x 120 DPI)